sciendo
Polish Journal of Medical Physics and Engineering
The Journal of Polish Society of Medical Physics
ISSN 1898-0309, doi: 10.2478/pjmpe-2024-0028
December 2024
Vol 30, Issue 4

Scientific Paper

Prediction of vertebral body mechanical parameters using opportunistic CT data

Eugeniusz ROKITA [1,ABCDF], Grzegorz TATOŃ [1,BCEF,*]

[1]*Faculty of Medicine, Chair of Physiology, Department of Biophysics, Jagiellonian University Medical College, Kraków, Poland*
[*]*Corresponding author: Prof. Grzegorz Tatoń; g.taton@uj.edu.pl*

(received 1 August 2024; revised 15 November 2024; accepted 3 December 2024)

Abstract

Introduction: The purpose of the study was to test a method describing the mechanical properties of bone using clinically available CT data.

Material and Methods: The samples, 50 L3 vertebrae taken from males 22 to 81 years old, were examined with dual-energy X-ray absorptiometry and quantitative CT. An analysis of CT images and their image histograms was performed. The greyscale means – XC_1, XC_2, their standard deviations – SD_1, SD_2, and the areas under the curves – X_1, X_2 characterizing the organic matrix and bone material, respectively, were calculated by fitting two Gaussian functions. The compression tests were performed to determine the elastic modulus (E), ultimate stress (σ_{max}), ultimate strain, and the ratio of work to fracture and the volume of the vertebra.

Results: It was found that E and σ_{max} were most precisely described by the parameter related to the trabecular bone density (XC_2) obtained from the histogram analysis. Using the linear model, the coefficient of determination (R^2) equals to 0.706 and 0.846 for E and σ_{max}, respectively. For volumetric (vBMD) and areal bone mineral density (aBMD), R^2 is 0.641 and 0.208 for E, while for σ_{max} equals 0.784 and 0.356. After correction of vBMD using the histogram parameters R^2 for E and σ_{max} rise to 0.692 and 0.835, respectively.

Conclusions: The superiority of the new method of E and σ_{max} estimation based on clinically available CT data was confirmed. The proposed method does not require calibration and predicts the mechanical parameters of the vertebrae more precisely than vBMD or aBMD separately.

Keywords: human vertebra; CT examination; image histogram analysis; prediction of mechanical properties; opportunistic screening.

Introduction

Vertebral fractures, the most common osteoporosis-related fracture, are the result mainly of a decrease in the stiffness and strength of bone tissue.[1] Therefore, the proper evaluation of the mechanical parameters of the bone and the determination of the fracture risk (FR) are an important issue. Direct measurement of bone mechanical properties is not possible in clinical practice; the mechanical strength of bone must be estimated indirectly. The standard diagnostic approach, unchanged for several decades, consists of determining the bone mineral density (BMD) and more precisely the areal bone mineral density (aBMD) using dual-energy X-ray absorptiometry (DXA), as it is a low-radiation and non-expensive technique. For diagnostic purposes, the aBMD results are compared with the values of the young population (T-score).[2]

Since aBMD-based test can only provide a rough understanding of how much weaker bones have become, numerous attempts have been made to develop more accurate diagnostic methods. Trials have been carried out to replace or supplement aBMD determinations with measurements of the geometry, microarchitecture, and volumetric BMD (vBMD) of bones using quantitative computed tomography (QCT), peripheral QCT, micro-CT, or a combination of these methods.[3-8] Of course, micro-CT is only used diagnostically for bone biopsies, but the method is not and will never become widely used.

Another way to improve diagnostic efficiency is to apply advanced mathematical methods to analyze two-dimensional (2D) or three-dimensional (3D) images of vertebral bodies. Bone strength calculations are made using the finite element method (FE). To perform the FE simulations, both micro- and macro-mechanical models are constructed using CT data.[9-10] There is also a tendency to use textural descriptors for the

Authors' contribution:
A – Research concept and design, B – Collection and/or assembly of data, C – Data analysis and interpretation, D – Writing the article, E – Critical revision of the article, F – Final approval of the article.

characterization of 2D CT images without requiring stringent segmentation of the individual trabecula.[11] Similarly, texture analysis can be applied to DXA images by computing the trabecular bone score (TBS).[12] In addition, more computer-advanced studies of trabecular architecture measurements from DXA-derived 3D models were published.[13]

Recently, two novel approaches are being tested to determine the mechanical properties of bone. First, as in other areas of medicine, radiomic features of CT images and artificial intelligence-based (AI) image analyses have been used to differentiate between normal and pathologically altered bones.[10,13-16] Second, vBMD is determined with CT acquired for other reasons (opportunistic CT) by converting the HU (Hounsfield Unit) scale using the scanner-specific conversion equation, calculated by asynchronous calibration.[17-21]

Based on the authors' knowledge, none of the diagnostic approaches described above have been widely accepted in clinical practice. The question arises as to whether it is possible to determine the mechanical parameters of the bones based on opportunistic CT data with higher precision than in the methods currently used.

The purpose of this study is to test a new method to describe the mechanical properties of bones based on clinically available CT data. The usefulness of the method for opportunistic CT data analysis is also discussed.

Material and Methods

The study comprises a reanalysis of pre-existing data acquired in previous experiments.[22-25] Approval for this reanalysis was not necessary due to the retrospective and deidentified nature of the data. The primary study was performed on 50 cadaveric L3 vertebrae taken from males aged 22 to 81 years (mean ± SD, 49 ± 15). The material studied was limited to male vertebra samples to eliminate gender-specific impacts on BMD.[26] All cadavers were included without bone disease screening because a complete medical history was not available for all subjects.

The following is a brief description of the experiment that was originally performed. Immediately after removal, the samples were placed in a methacrylate body phantom filled with 0.9% NaCl solution to simulate physiological conditions. The samples were examined with DXA using a Lunar DPX-IQ densitometer (Lunar, Madison, USA), following standard procedures applied to humans. A Siemens Somatom Sensation 10 CT unit (Siemens, Erlangen, Germany) was used for CT examinations (120 kV, 120 mAs, slice thickness: 0.6 mm). A 75×75 mm^2 region of interest (ROI) and a matrix of 512×512 resulted in a pixel size of 146×146 μm^2 in the scan plane. CT data was also used to determine the BMD of the trabecular bone region (vBMD) within the vertebral bodies. The Siemens Osteo-CT procedure (Siemens, Erlangen, Germany) was applied for the determination of vBMD.

Finally, DICOM data acquired in CT examinations were reconstructed in 3D, using software developed in our laboratory. 3D images were used to measure the linear, areal, and volumetric dimensions of vertebral bodies.[23] Subsequently, 3D images were applied to identify vertebral fractures according to the method of Genant et al.[27]

After CT scans, all specimens were subjected to axial compression to failure on an Instron 5566 testing machine (Instron, High Wycombe, UK).[24-25] The definitions of the parameters determined are given in **Figure 1**.

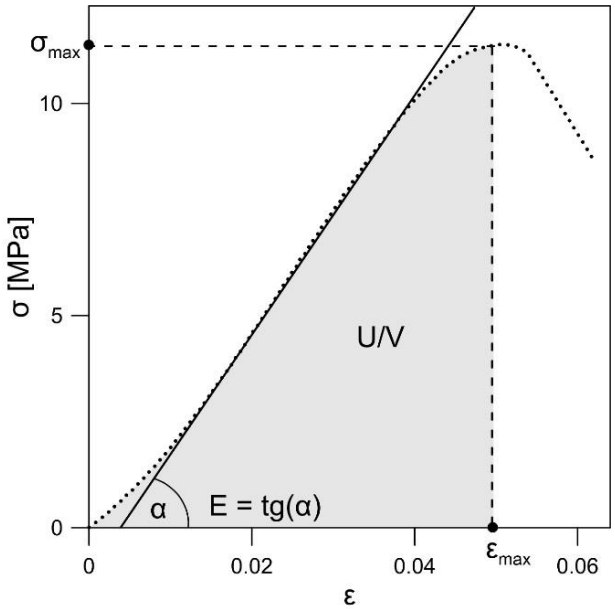

Figure 1. Typical stress-strain curve obtained during the compression test of the human L3 vertebral body with the definitions of the mechanical parameters. E, σ_{max}, ε_{max} and U/V are Young's modulus, maximum stress, ultimate strain, and the fracture work (U) divided by the volume of the vertebral body (V), respectively.

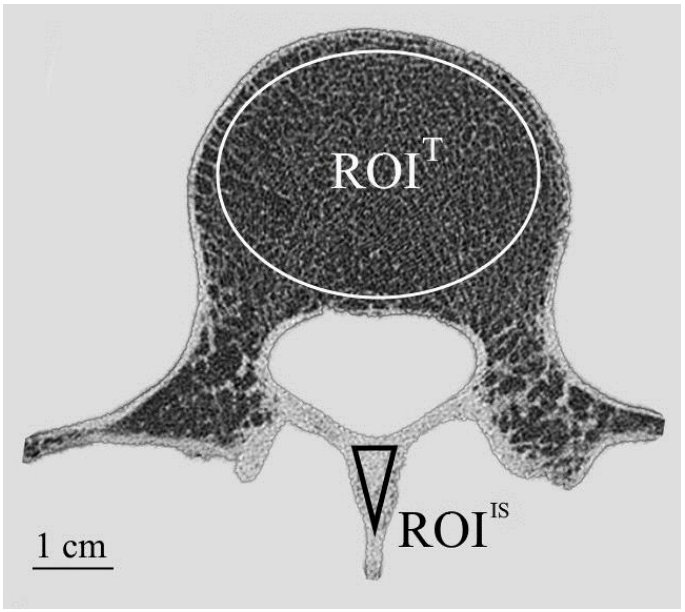

Figure 2. Representative 2D CT image of human vertebral cross sections. The regions of interest used for the calculation of the trabecular bone parameters (ROI^T) and for the normalization of the ROI^T histogram (ROI^{IS}) are marked.

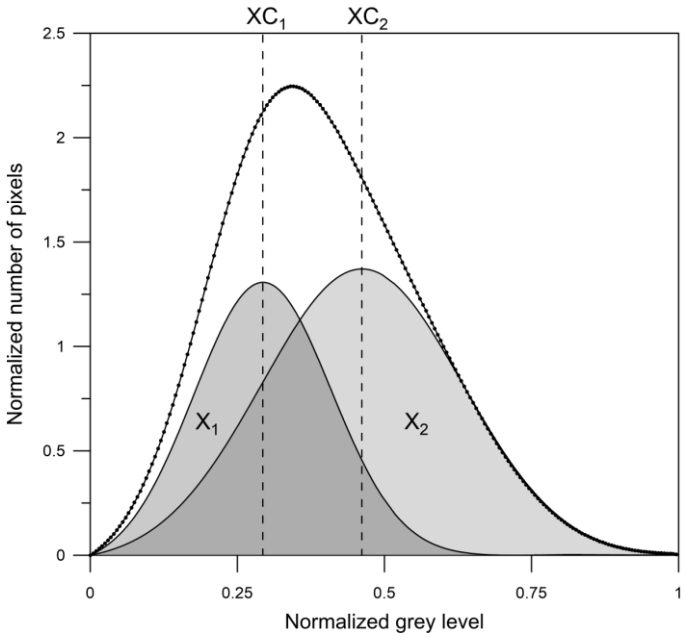

Figure 3. Example of the normalised global histogram of the relative grey level distribution for a vertebral body. X_1 and X_2 are the areas, and XC_1 and XC_2 mark the positions of the maxima of 2 Gaussian functions. The black dots represent the experimental points (every second point is shown). Solid lines present Gaussian functions.

As the new step in 2D image analysis (**Figure 2**), the grey level (GL) histogram was constructed for the region of interest within the trabecular bone part of the vertebral body - ROI^T (GLT). The histogram was normalized using the average GL obtained for the histogram of the region of interest within the spinous process of vertebrae, ROI^{IS} (GLC), and the relative grey level histogram (RGL = GLT/GLC) was calculated. ROI^T and ROI^{IS} were manually selected by placing an ellipse and a triangle in the vertebral body and the spinous process of the vertebra, respectively. Next, all RGL histograms (~40 sections for each vertebra) were pooled together and the global histogram for the vertebral body was prepared. The global histogram was normalized (area = 1) and the average relative grey level (<RGL>) was calculated. It should be noted that vBMD can be determined from the histogram using <RGL>. However, we need to apply the calibration procedure after <RGL> estimation. Finally, two Gaussian functions (**Figure 3**) were fitted to the RGL histogram. By applying this method, the global histogram was decomposed into two different classes, hereinafter referred to as the organic matrix and bone material (Appendix). Six parameters were obtained: means – XC_1 and XC_2, standard deviations – SD_1 and SD_2, and finally areas – X_1 and X_2. The indices '1' and '2' mark the organic matrix and bone material, respectively. Due to the normalization of the histogram, $X_1 + X_2 = 1$, the number of independent parameters is five.

It should be noted that ROI^T of a 2D image (**Figure 2**) contains ~$2 \cdot 10^4$ pixels. Therefore, the global histogram for a vertebral body is based on several hundred thousand points. The histogram skewness is positive in all cases and ranges from 0.26 to 1.19. Therefore, two Gaussian distributions were fitted to reproduce the experimental data. Unambiguously, fitting the two Gaussian curves provides an excellent reproduction of the experimental data ($R^2 > 0.999$).

Results are presented as parameter ranges, and as mean ± SD. Prior to the analyses, a normal distribution check was performed for all data (Shapiro-Wilk test, $p < 0.05$). Relationships between parameters and age were investigated using the Pearson correlation coefficient (r) and its significance level (p). The statistical significance of the differences in the correlation coefficients was tested using the procedure proposed by Steiger.[28] The Student's t-test was applied to compare mean values. Different regression models (linear – $a \cdot x+b$, parabolic – $a \cdot x^2+b \cdot x+c$, logistic – $a/(1 + b \cdot \exp(-c \cdot x))$, and power – $a \cdot x^b$) were constructed for the selection of variables explaining the results of mechanical tests. The best model was selected using the coefficient of determination (R^2) as well as the AIC (Akaike Information Criterion) and BIC (Bayesian Information Criterion) tests. OriginPro 2020 software (Northampton, MA, USA) was used to perform statistical analysis.

Results

An example of the 3D CT image of the vertebral body is presented in **Figure 4**, while the 2D CT images of the ROI^T extracted from the vertebral sections are presented in **Figure 5**. The linear, areal, and volumetric dimensions of the vertebral bodies, extracted from 3D images, were given elsewhere.[23] To quantify the trabecular bone architecture, 2D images were applied. The usefulness of ~30 parameters for characterization of trabecular bone architecture has been checked.[29-31] A detailed description of these results is beyond the scope of this paper. Two geometric parameters (A - axial cross-section area at the narrowest site of the vertebral body; H - the average height of the vertebral body) and one descriptor of trabecular architecture (BV/TV – bone volume/total volume) were selected as examples of for further considerations.

The first aim of the studies was to improve the description of the mechanical properties of the vertebra (FR prediction) based on the available clinical data. Previously obtained results[23-25,29-31] and the research described in this paper allowed to determine several dozens of parameters that describe the geometry, architecture, density, and mechanical properties of the vertebral body. Therefore, it is necessary to adopt a criterion that allows the initial selection of experimental data.

In the paper, it is assumed that the natural ageing process is observed in the absence of fractures, since the bone fracture changes the parameter values in a way that is impossible to quantify. As a result, it was decided to determine the relationship between mechanical parameters and clinical data only for unbroken vertebrae. According to the Genant et al. classification[27], vertebrae with mild (grade 1) or larger deformities were considered as fractured. In the group of 50 cases studied, 18 did meet the selection criteria. The use of stringent criteria limited the size of the study group but ensures that the group for which there are only physiological changes depending on age is analyzed.

Table 1 shows the ranges of selected parameters and their correlations with age. The values of all parameters are in line with those already published.[32-33] Among the parameters that characterize the mechanical properties of vertebrae, σ_{max}, E and U/V correlate with age. For ultimate strain (ε_{max}), the correlation is not observed ($r = -0.38$, $p = 0.115$). Assuming that the vertebral body is a cylinder with the volume $V = A \cdot H$, made of a material that meets Hook's law ($\sigma = E \cdot \varepsilon$), one can calculate (**Figure 1**) the energy storage in the elastic body as $U/V \approx (\frac{1}{2}) \cdot \sigma_{max} \cdot \varepsilon_{max}$ while $\varepsilon_{max} \approx \sigma_{max}/E$. Finally, we get $U/V \approx (\sigma_{max})^2/2E$. The approximations are valid, since the vertebral body resembles a ceramic material. The maximum stress appears only a little into the non-linear elastic region. The accuracy of the approximation used is confirmed by a very strong correlation between U/V and $(\sigma_{max})^2/2E$ ($r = 0.94$, $p < 0.001$). The relations described above make it possible to limit the description of the mechanical property of a vertebral body to two parameters. Furthermore, there are significant differences for young (≤ 55 y) and old (> 55 y) individuals in the case of average σ_{max} (11.4 ± 2.0 vs 6.8 ± 2.6 MPa, $p < 0.001$) and E (326 ± 36 vs 202 ± 70 MPa, $p < 0.001$).

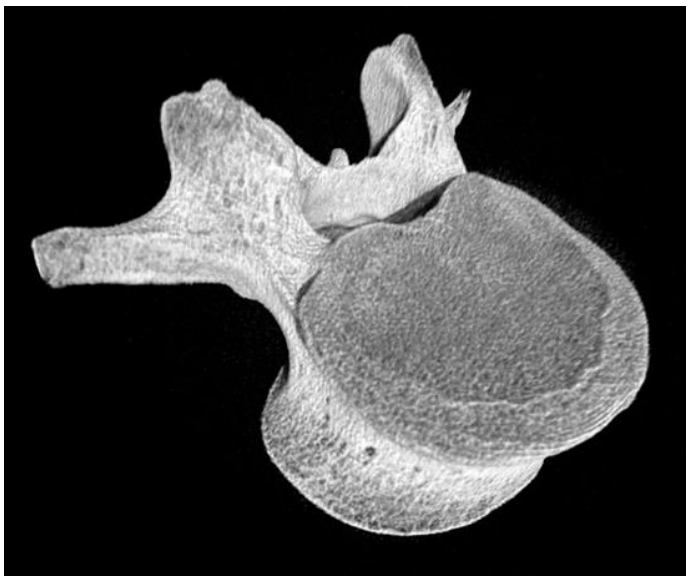

Figure 4. Representative 3D CT image of the human L3 vertebral body.

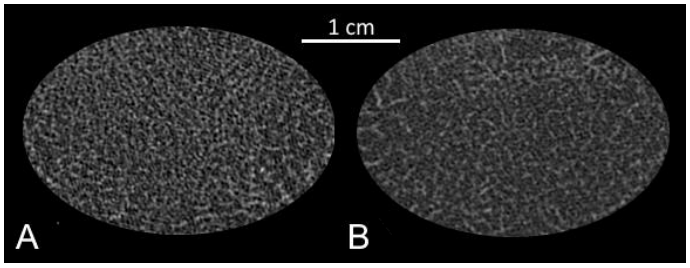

Figure 5. 2D raw CT images of the ROI^T regions for human L3 vertebral bodies collected from 25-year-old subject (A) and 66-year-old subject (B).

Table 1. The ranges of values of the parameters describing selected properties of the L3 vertebral body. The correlation coefficients of the parameters with the age (r) and p values are given. For the definition of symbols, see text.

Parameter	Range	r	p
E (MPa)	141 ÷ 394	-0.77	<0.001
σ_{max} (MPa)	3.83 ÷ 13.8	-0.74	<0.001
U/V (MPa)	0.11 ÷ 0.41	-0.64	0.005
A (cm^2)	10.9 ÷ 18.2	0.75	<0.001
H (cm)	1.97 ÷ 3.05	-0.74	<0.001
BV/TV	0.09 ÷ 0.30	-0.71	0.001
vBMD (g/cm^3)	0.051 ÷ 0.169	-0.65	0.004
aBMD (g/cm^2)	0.74 ÷ 1.53	-0.40	0.110
X_2	0.39 ÷ 0.72	-0.55	0.018
XC_2	0.31 ÷ 0.62	-0.69	0.001
SD_2	0.12 ÷ 0.17	-0.75	<0.001

Regarding vertebral geometry, data analysis confirms general observations. The L3 vertebrae show a trend towards a decrease in height and an increase in the area of the axial cross section with age, while the volume of the body does not change with age ($r = 0.22$, $p = 0.382$).

Most of the parameters that characterize the mineral content of the vertebral body correlate with age. This applies both to 3 parameters obtained from histogram analysis (X_2, XC_2, SD_2) and to the parameters commonly used in the description of trabecular bone density (vBMD) or to the parameter related to bone density (BV/TV). Unlike bone material, the parameters that characterize the organic matrix (XC_1, SD_1) vary to a very narrow extent ($0.29 \div 0.35$ and $0.08 \div 0.12$, respectively) and do not correlate with age ($r = -0.46$, $p = 0.057$ and $r = -0.27$ $p = 0.271$, respectively). XC_1 and SD_1 are also not correlated with age ($r = 0.006$, $p = 0.982$). It should be emphasized that aBMD does not correlate with age in cases without fracture. This parameter will be further considered, as it is the most widely used to assess fracture risk in clinical practice.

As the first step in describing the mechanical parameters by CT data, a linear regression model was used. Partial correlations between mechanical parameters and another selected vertebral body parameters that are clinically available were calculated to eliminate the effect of ageing on the relationship. The results are given in **Table 2**.

The geometrical parameters (A, H) were not included in **Table 2** due to weak correlations with σ_{max} and E ($r < 0.40$). The geometry of vertebrae is probably useful for the differentiation of broken/unbroken vertebrae, but it does not provide information on the mechanical parameters of the vertebrae. The same applies to BV/TV, X_2, and SD_2 ($r < 0.5$) while the $vBMD/X_2$ ratio was also included (Appendix). The data in **Table 2** confirm that XC_2 and $vBMD/X_2$ are the best predictors of the mechanical parameters.

Finally, attempts were made to describe the relationship between mechanical parameters and clinically available quantities using the nonlinear models listed above. Based on the values of R^2, ACI, and BCI, it turned out that the use of a parabolic model provides the best description of E and σ_{max} (**Table 3**). The results of the power and logistic models are practically identical to those of the linear model. It should be noted that up to 90 % of the variation in the outcome variables is explained by the parabolic model, while for the linear model, the values R^2 are ~10% lower.

The superiority of the parabolic model for the XC_2 variable can be achieved by using a linear model for the $XC_2 \cdot SD_2$ parameter (Appendix). It is pure mathematics, based on the strong XC_2 - SD_2 correlation. This provides a few percent improvement in the R^2 values (**Table 3**) in comparison of the XC_2 based linear model.

Table 2. Partial correlations (effect of age has been eliminated) between mechanical parameters and parameters characterizing the density of the L3 vertebral body. The values of the partial correlation coefficient and p are given. For the definition of symbols, see text.

Parameter	E	σ_{max}	vBMD	aBMD	XC_2
σ_{max}	0.75 0.001	1			
vBMD	0.62 0.008	0.79 <0.001	1		
aBMD	0.26 0.315	0.49 0.045	0.77 <0.001	1	
XC_2	0.67 0.004	0.84 <0.001	0.82 <0.001	0.59 0.013	1
$vBMD/X_2$	0.71 0.001	0.86 <0.001	0.87 <0.001	0.59 0.012	0.86 <0.001

Table 3. Coefficients of determination for the linear (Lin) and parabolic (Par) models describing the stiffness (E) and strength (σ_{max}) of the L3 vertebral body. All independent variables can be extracted from an opportunistic analysis of CT data. For the definition of symbols, see text.

Parameter	E (MPa)		σ_{max} (MPa)	
	Lin	Par	Lin	Par
BV/TV	0.554	0.558	0.720	0.731
vBMD (g/cm^3)	0.641	0.700	0.784	0.844
aBMD (g/cm^2)	0.208	0.212	0.356	0.369
XC_2	0.706	0.795	0.846	0.893
$vBMD/X_2$	0.692	0.737	0.835	0.856
$XC_2 \cdot SD_2$	0.768	- -	0.865	- -

Discussion

The goal of all studies relating bone density and structure to bone strength and stiffness is to predict FR in a specific patient using clinically available data. In these retrospective studies, the mechanical characteristics of the vertebra were assessed, in fact, by opportunistic CT data analysis. It was assumed that the most important parameter characterizing the FR is σ_{max}, as it denotes when fractures really occurs. With E in addition, it is possible to estimate the values of U/V and ε_{max}. The selection of parameters matches the widely accepted opinion that strength (σ_{max}) and stiffness (E) are the best quantities to define the "health" of bone. The values given in **Tables 2** and **3** confirm the positive proportionality of different measures of BMD with bone strength and stiffness, which has been repeatedly demonstrated over many years.[32-33] The results clearly confirm that aBMD does not offer a good assessment of the mechanical properties. In contrast to aBMD, vBMD provides a better prediction of mechanical strength. The determination of vBMD requires a CT application, which significantly limits the use of this parameter in clinical practice. It should also be noted that the prediction of osteoporosis using aBMD and vBMD does not overlap. According to the criteria of aBMD for the diagnosis of osteoporosis (T-score < - 2.5),[34] samples subjected to studies can be classified as normal/osteopenic in 15 cases and as

osteoporotic in 3 cases. Using the vBMD values (< 0.080 g/cm^3) for classification,[35] we get 13 and 5 cases, respectively.

In many studies, the quantities that characterize the vertebral microstructure and the thickness of the cortical bone are also calculated based on clinical CT data. This approach is in line with the commonly accepted opinion that to fully characterize the mechanical properties of vertebrae, it is necessary to supplement density measurements with a quantitative description of the trabecular architecture and/or cortical thickness.[36] However, in clinical practice, the parameters that characterize the architecture of the trabecular bone are not used. The basic problem of bone microstructure studies is the problem of the limited resolving power of CT images obtained in clinical trials.[37] Although modern CT scanners achieve an isotropic resolution at the level of ~0.5 mm,[38] for standard clinical examination, a minimum in-plane resolution of the order of 1 mm and a slice thickness > 1 mm is used. Therefore, given typical dimensions of the trabecula, the image resolution seems to be the borderline for a quantitative determination of trabecular architecture.

The common feature of all methods currently tested to replace or supplement density measurements is that instead of directly measuring microstructural parameters, there is a tendency to use textural descriptors to characterize the trabecular architecture.[11,39] It should be noted that the texture analysis is based on the quantitative description of image grey-level variations without biophysical background. In our study, we proposed a new, very simple method instead of trabecular architecture description or texture analysis.

Our approach uses a patient-specific phantom-less normalization method (synchronous internal calibration). The technique uses the patient's own internal tissue (ROI^{IS} – **Figure 2**) as normalization material. Typically, adjacent internal tissue (blood or fat) and air are used for normalization.[40] It should be noted that the ROI^{T} and ROT^{IS} regions are close to each other (~cm). Therefore, the influence of all parasitic effects characteristic for CT examination is practically eliminated. The use of RGL is a simple method to limit the influence of the scanner operating parameters (collimation, X-ray tube kV_P, slice thickness), the radiation hardening effect, the effect of intravenous contrast on bone attenuation, the image processing method, etc.

The quantitative description of the density of the trabecular bone is based on image histogram analysis. The proposed histogram analysis allows for the separation of the organic matrix and bone material. Additionally, the contribution of the organic phase (X_1) and the mineral phase (X_2) is separated and the quantities that measure the density of the individual phases (XC_1 and XC_2) are determined. Simple visual inspection of 2D images (**Figure 5**) confirms the commonly known effect that X_1 increases, while X_2 decreases with age. The observed variations in XC_2 and SD_2 with age (**Table 1**) may be related to changes in the balance between bone formation and resorption. However, the exact interpretation requires further investigation.

The XC_2 parameter allows for the best prediction of the mechanical characteristics of all the quantities tested. **Figure 6** shows the modulus of elasticity (E) and ultimate stress (σ_{max}) versus XC_2. The very good prediction of E ($R^2 = 0.706$, $r = 0.84$, $p < 0.001$) and the excellent description of σ_{max} ($R^2 = 0.846$, $r = 0.92$, $p < 0.001$) using the linear model are clearly visible. Consistently, the replacement of vBMD with $vBMD/X_2$ improves correlations with mechanical parameters (**Table 3**).

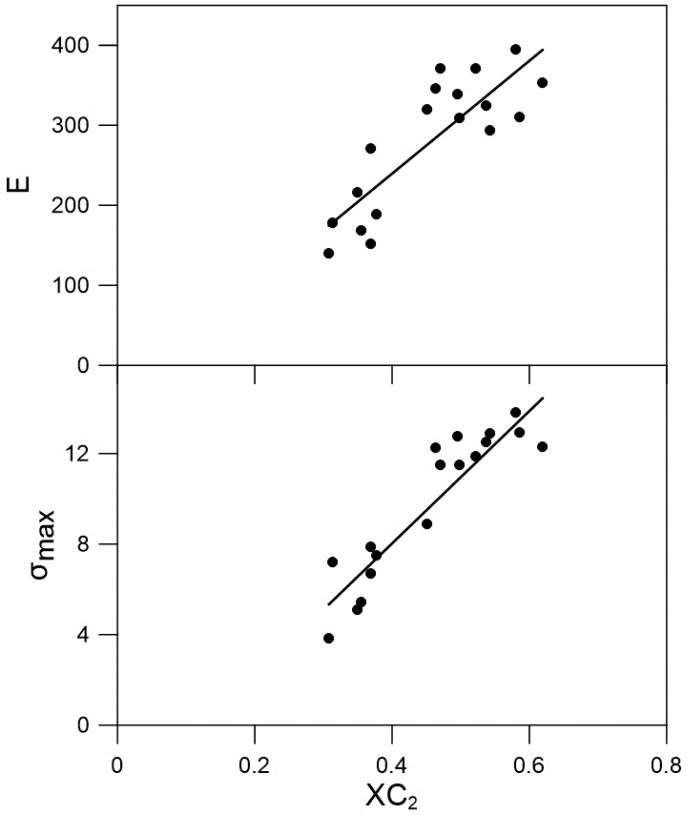

Figure 6. Elastic modulus (E - MPa) and ultimate stress (σ_{max} - MPa) vs bone material density measure (XC_2) extracted from histogram analysis. The solid line represents the linear regression model (r = 0.84 and 0.92, p < 0.001 for E and σ_{max}, respectively).

Trabecular bone is an example of a class of materials called cellular solids. Cellular solids are made up of cells with solid edges or faces that are piled together to fit a certain space. Many cellular solids have been manufactured (honeycomb materials, polymer foams) for different industrial applications. New materials are synthesized, and their properties are studied in many laboratories. The experimental results and theoretical calculations clearly prove the nonlinear dependence of mechanical parameters on density[41-43] for cellular solid material. Therefore the nonlinear dependence between E or σ_{max} and the density has been checked. The results obtained confirm that the best description is provided by a parabolic model for XC_2 and the linear model for the product of two correlated parameters: XC_2 and SD_2. Small differences between the results of the

parabolic and linear models (< 10%) allow, in our opinion, the use of the linear model in clinical practice. Additionally, one should pay attention to the certain regularity observed in the processing of the results. The ranges of parameter changes exhibited by the vertebral bodies are low for patients over 50 years of age (less than factor 4 – **Table 1**). It is known from mathematics that small changes in variable values can be very accurately described with linear models.

It is worth highlighting the additional advantage of the proposed approach. The values of histogram parameters seem to be weakly dependent on image resolution. A poorer resolving power means fewer points in the global histogram. The histograms analysed in this paper contained several hundred thousand points. Reducing the number of points by a factor of ~25 means that the global histogram is still based on several tens of thousands of points. For so many points, the histogram parameters can be determined with very good accuracy. The tests performed confirmed that the five-fold deterioration of image resolution (pixel - 730×730 μm^2) changes the parameters by less than 2%. However, the problem of image resolution requires additional research using clinical CT data.

Considering the opportunistic determinations of vBMD,[18-21] in a routine approach, the vBMD values are calculated by converting HU using scanner-specific conversion equations, including a correction offset for contrast-enhanced CT scans. It should be noted that the calculation of vBMD is important since we can use the standardized diagnostic thresholds for diagnostic purposes.[35] The proposed histogram analysis method also allows for the determination of vBMD using <RGL> values. As expected, a very strong correlation was observed between vBMD and <RGL> ($r = 0.97$, $p < 0.001$). It can be further concluded that in the case of opportunistic determination of vBMD, calculations should be supplemented with histogram analysis and not vBMD but vBMD/X_2 should be used.

It should be clearly emphasized that the proposed method of assessing the mechanical parameters of the vertebrae can be used for CT images obtained in various clinical trials. There is no need to perform a calibration procedure, nor does it need to be precisely known the parameters of the scanner operation. The currently proposed methods of analyzing CT images of bones, similar to many other branches of medicine, based on the use of AI methodology, do not offer such possibilities. The published works[44-45] concern studies of animal material using micro-CT devices, and their duplication in clinical studies is not possible due to the way in which neural networks are trained. In order to use the AI methodology, it is necessary to develop a new approach that will not be a simple extension of the methods used. The studies carried out have several limitations. First, the sample size should be larger. We have analysed 50 vertebral bodies, but the most interesting results were obtained for the group of 18 cases. Increasing the number of subjects studied will probably not change the observed relationships that appear to be unambiguous. The next drawback is that the examinations were performed in vitro. Therefore, the images analysed have provided a better resolution and quality than the clinical CT images. Although the test performed showed that the results of the histogram analysis depended weakly on the image resolution, the problem requires further studies. Finally, we should also consider the limitations associated with the lack of standardized diagnostic thresholds for XC_2 and vBMD/X_2.

Conclusions

The paper describes a reanalysis of previously acquired CT data, i.e. opportunistic analysis. Several dozens of parameters describing human vertebra were tested as predictors of mechanical properties and fracture risk (FR). A new method for predicting FR was proposed using the parameter extracted from the CT image histogram. In fact, the proposed approach offers a description of the mechanical parameters through the bone density estimator. Despite some limitations, it seems that the proposed parameter (XC_2) is potentially promising for the opportunistic analysis of chest, abdomen, pelvis, and spine CT scans. In the case of opportunistic determination of vBMD, a histogram analysis should be performed and vBMD/X_2 calculated.

References

1. Hernlund E, Svedbom A, Ivergård M, et al. Osteoporosis in the European Union: medical management, epidemiology and economic burden. A report prepared in collaboration with the International Osteoporosis Foundation (IOF) and the European Federation of Pharmaceutical Industry Associations (EFPIA). Arch Osteoporos. 2013;8:136. https://doi.org/10.1007/s11657-013-0136-1
2. Aibar-Almazán A, Voltes-Martínez A, Castellote-Caballero Y, et al. Current status of the diagnosis and management of osteoporosis. Int J Mol Sci. 2022;23:9465. https://doi.org/10.3390/ijms23169465
3. Nethander M, Pettersson-Kymmer U, Vandenput L, et al. BMD-related genetic risk scores predict site-specific fractures as well as trabecular and cortical bone microstructure. J Clin Endocrinol Metab. 2020;105:e1344–e1357. https://doi.org/10.1210/clinem/dgaa082
4. Shepherd JA, Schousboe JT, Broy SB, et al. Executive summary of the 2015 ISCD position development conference on advanced measures from DXA and QCT: fracture prediction beyond BMD. J Clin Densitom. 2015;18:274-286. https://doi.org/10.1016/j.jocd.2015.06.013

5. Silva BC, Broy SB, Boutroy S, et al. Fracture risk prediction by non-BMD DXA measures: the 2015 ISCD official positions, part 2: trabecular bone score. J Clin Densitom. 2015;18:309-330. https://doi.org/10.1016/j.jocd.2015.06.008
6. Adami G, Biffi A, Porcu G, et al. A systematic review on the performance of fracture risk assessment tools: FRAX, DeFRA, FRA-HS. J Endocrinol Invest. 2023;46:2287-2297. https://doi.org/10.1007/s40618-023-02082-8
7. Soldati E, Rossi F, Vicente J, et al. Survey of MRI usefulness for the clinical assessment of bone microstructure. Int J Mol Sci. 2021;22:2509. https://doi.org/10.3390/ijms22052509
8. Akhter MP, Recker RR. High resolution imaging in bone tissue research-review. Bone. 2021;143:115620. https://doi.org/10.1016/j.bone.2020.115620
9. Johannesdottir F, Allaire B, Bouxsein ML. Fracture prediction by computed tomography and finite element analysis: current and future perspectives. Curr Osteoporos Rep. 2018;16:411-422. https://doi.org/10.1007/s11914-018-0450-z. Erratum in: Curr Osteoporos Rep. 2022;20:364. https://doi.org/10.1007/s11914-022-00724-z
10. Fleps I, Morgan EF. A Review of CT-based fracture risk assessment with finite element modeling and machine learning. Curr Osteoporos Rep. 2022;20:309-319. https://doi.org/10.1007/s11914-022-00743-w
11. Gebre RK, Hirvasniemi J, Lantto I, et al. Discrimination of low-energy acetabular fractures from controls using computed tomography-based bone characteristics. Ann Biomed Eng. 2021;49:367-381. https://doi.org/10.1007/s10439-020-02563-4
12. Silva BC, Leslie WD, Resch H et al. Trabecular Bone Score: A noninvasive analytical method based upon the DXA image. J Bone Mineral Res. 2014;29:518-530. https://doi.org/10.1002/jbmr.3218
13. López Picazo M, Humbert L, Di Gregorio S, et al. Discrimination of osteoporosis-related vertebral fractures by DXA-derived 3D measurements: a retrospective case-control study. Osteoporosis Int. 2019;30:1099-1110. https://doi.org/10.1007/s00198-019-04894-y
14. Xie Q, Chen Y, Hu Y, et al. Development and validation of a machine learning-derived radiomics model for diagnosis of osteoporosis and osteopenia using quantitative computed tomography. BMC Med Imaging. 2022;22:140. https://doi.org/10.1186/s12880-022-00868-5
15. Xue Z, Huo J, Sun X, et al. Using radiomic features of lumbar spine CT images to differentiate osteoporosis from normal bone density. BMC Musculoskelet Disord. 2022;23:336. https://doi.org/10:1186/s12891-022-05309-6
16. Yan J, Lai Y, Xu Y, et al. Editorial: Artificial intelligence-based medical image automatic diagnosis and prognosis prediction. Front Phys. 2023;11:1210010. https://doi.org/10.3389/fphy.2023.1210010
17. Valentinitsch A, Trebeschi S, Kaesmacher J, et al. Opportunistic osteoporosis screening in multi-detector CT images via local classification of textures. Osteoporos Int. 2019;30:1275-1285. https://doi.org/10.1007/s00198-019-04910-1
18. Leonhardt Y, May P, Gordijenko O, et al. Opportunistic QCT bone mineral density measurements predicting osteoporotic fractures: a use case in a prospective clinical cohort. Front Endocrinol. 2020;11:586352. https://doi.org/10.3389/fendo.2020.586352
19. Löffler MT, Jacob A, Valentinitsch A, et al. Improved prediction of incident vertebral fractures using opportunistic QCT compared to DXA. Eur Radiol. 2019;29:4980-4989. https://doi.org/10.1007/s00330-019-0618-w
20. Boutin RD, Hernandez AM, Lenchik L, et al. CT phantom evaluation of 67,392 American College of Radiology accreditation examinations: implications for opportunistic screening of osteoporosis using CT. Am J Roentgenol. 2021;216:447-452. https://doi.org/10.2214/AJR.20.22943
21. Lenchik L, Weaver AA, Ward RJ, et al. Opportunistic screening for osteoporosis using computed tomography: State of the art and argument for paradigm shift. Curr Rheumatol Rep. 2018;20:74. https://doi.org/10.1007/s11926-018-0784-7
22. Tatoń G, Rokita E, Rok T, et al. Oversampling in the computed tomography measurements applied for bone structure studies as a method of spatial resolution improvement. Pol J Radiol. 2012;77:14-18. https://doi.org/10.12659/pjr.882965
23. Tatoń G, Rokita E, Wróbel A. Application of geometrical measurements in the assessment of vertebral strength. Pol J Radiol. 2013;78:15-18. https://doi.org/10.12659/PJR.883942
24. Tatoń G, Rokita E, Wróbel et al. Combining areal DXA bone mineral density and vertebrae postero-anterior width improves the prediction of vertebral strength. Skeletal Radiol. 2013;42:1717-1725. https://doi.org/10.1007/s00256-013-1723-3
25. Tatoń G, Rokita E, Korkosz et al. The ratio of anterior and posterior vertebral heights reinforces the utility of DXA in assessment of vertebrae strength. Calcif Tissue Int. 2014;95:112-121. https://doi.org/10.1007/s00223-014-9868-1
26. Alswat KA. Gender disparities in osteoporosis. J Clin Med Res. 2017;9:382-387. https://doi.org/10.14740/jocmr2970w
27. Genant HK, Wu CY, Kuijk C, et al. Vertebral fracture assessment using a semiquantitative technique. J Bone Miner Res. 1993;8:1137-1148. https://doi.org/10.1002/jbmr.5650080915
28. Steiger JH. Tests for comparing elements of a correlation matrix. Psychol Bull. 1980;187:245-251. https://doi.org/10.1037/0033-2909.87.2.245
29. Tabor Z, Rokita E. Comparison of trabecular bone architecture in young and old bone. Med Phys. 2000;27:765-772. https://doi.org/10.1118/1.598981

30. Kubik T, Pasowicz M, Tabor Z, et al. Optimizing the assessment of age-related changes in trabecular bone. Phys Med Biol. 2002;47:1543-1553. https://doi.org/10.1088/0031-9155/47/9/309
31. Tabor Z. Quantifying quality of trabecular bone from low-resolution images. Nalecz Institute of Bio-cybernetics and Biomedical Engineering Polish Academy of Science, Warsaw, 2009; 16-56.
32. Karim L, Hussein AI, Morgan EF, et al. The mechanical behavior of bone. In: Marcus R, Feldman D, Dempster DW, Luckey M, Cauley JA, editors. Osteoporosis. Oxford: Academic Press; 2013. p. 431-452. https://doi.org/10.1016/B978-0-12-415853-5.00019-4
33. Boskey AL, Imbert L. Bone quality changes associated with aging and disease: a review. Ann N Y Acad Sci. 2017;1410:93-106. https://doi.org/10.1111/nyas.13937
34. Jain RK, Vokes T. Dual-energy X-ray absorptiometry. J Clin Densitometry. 2017;20:291-303. https://doi.org/10.1016/j.jocd.2017.06.014
35. American College of Radiology. ACR-SPR-SSR practice guideline the performance of quantitative computed tomography (QCT) bone densitometry. 2013. Available at: https://www.acr.org/-/media/ACR/Files/Practice-Parameters/QCT.pdf?la=en (Accessed 12 April 2024).
36. Yamada S, Chiba K, Okazaki N, et al. Correlation between vertebral bone microstructure and estimated strength in elderly women: an ex-vivo HR-pQCT study of cadaveric spine. Bone. 2019;120:459-464. https://doi.org/10.1016/j.bone.2018.12.005
37. Liu Y, Wang L, Su Y, et al. CTXA hip: the effect of partial volume correction on volumetric bone mineral density data for cortical and trabecular bone. Arch Osteoporos. 2020;15:50. https://doi.org/10.1007/s11657-020-00721-8
38. Engelke K. Quantitative computed tomography – current status and new developments. J Clin Densitom. 2017;20:309-321. https://doi.org/10.1016/j.jocd.2017.06.017
39. Checefsky WA, Abidin AZ, Nagarajan MB, et al. Assessing vertebral fracture risk on volumetric quantitative computed tomography by geometric characterization of trabecular bone structure. Proc SPIE - Int Soc Opt Eng. 2016;9785:978508. https://doi.org/10.1117/12.2216898
40. Lee DC, Hoffmann PF, Kopperdahl DL, et al. Phantomless calibration of CT scans for measurement of BMD and bone strength-inter-operator reanalysis precision. Bone. 2017;103:325-33. https://doi.org/10.1016/j.bone.2017.07.029
41. Gibson LJ. Biomechanics of cellular solid. J Biomech. 2005;38:377-399. https://doi.org/10.1016/j.jbiomech.2004.09.027
42. Moeendarbary E, Harris AR. Cell mechanics: principles, practices, and prospects. Rev Syst Biol Med. 2014;6:371-388. https://doi.org/10.1002/wsbm.1275
43. Costanza G, Solaiyappan D, Tata ME. Properties, applications and recent developments of cellular solid materials: A review. Materials. 2023;16:7076. https://doi.org/10.3390/ma16227076
44. Coulombe JC, Mullen ZK, Lynch ME, et al. Application of machine learning classifiers for microcomputed tomography data assessment of mouse bone microarchitecture. MethodsX. 2021;8:101497. https://doi.org/10.1016/jmex.2021.101497
45. Kodama M, Takeuchi A, Uesugi M, at al. Machine learning super-resolution of laboratory CT images in all-solid-state batteries using synchrotron radiation CT as training data. Energy and AI. 2023;100305. https://doi.org/10.1016/j.egyai.2023.100305

Appendix

The biophysical background of the proposed approach is based on the assumption that the vertebral body is composed of two phases (organic matrix – 1 and bone material – 2). Using the rule of mixture, the following formula may be written:

$$\rho = \rho_1 \cdot v_1 + \rho_2 \cdot v_2 = \text{vBMD} \approx C \cdot (XC_1 \cdot X_1 + XC_2 \cdot X_2)$$

where ρ is density of trabecular bone (vBMD), ρ_1 and ρ_2 are densities of both phases while v_1 and v_2 are the normalized volume fractions ($v_1 + v_2 = 1$) and C is a constant. The parameters XC_1 and XC_2 are linearly related to the densities of the organic matrix and bone material. The X_1 and X_2 are normalized volume fractions of organic matrix and bone material. The SD_1 and SD_2 parameters reflect the distributions of bone material and organic matrix.

Additionally, the following approximation can be used:

$$\frac{\text{vBMD}}{X_2} = C \cdot \left(XC_1 \cdot \frac{X_1}{X_2} + XC_2\right) \approx C \cdot XC_2$$

The accuracy of the approximation is confirmed by a very strong correlation between vBMD/X_2 and XC_2 ($r = 0.90$, $p < 0.001$).

Note that a strong correlation of XC_2 and SD_2 was observed ($r = 0.70$, $p = 0.008$). Hence, there is a relationship ($SD_2 = C_1 \cdot XC_2 + C_2$) that results in:

$$\sigma_{max} = C_4(XC_2 \cdot SD_2) + C_5 = C_4(XC_2 \cdot (C_1 XC_2 + C_2) + C_5 = C_7(XC_2)^2 + C_8 XC_2 + C_9$$

where C_i are constants. The correctness of the approximation is confirmed by a very strong correlation of $XC_2 \cdot SD_2$ and $(C_7(XC_2)^2 + C_8 XC_2 + C_9)$, $R^2 = 0.95$.